Influence of Battery Downsizing and SOC Operating Window on Battery Pack Performance in a Hybrid Electric Vehicle

Nassim A. Samad, Youngki Kim, Jason B. Siegel and Anna G. Stefanopoulou
Department of Mechanical Engineering
University of Michigan
Ann Arbor, Michigan 48109
Email: {nassimab,youngki,sigeljb,annastef}@umich.edu

***Abstract*—This paper provides a parametric study for (1) downsizing a battery pack (reducing the number of battery cells), potentially reducing cost and weight; and (2) lowering the nominal operating SOC to reduce degradation. The downsized pack design with shifted SOC window is evaluated in a light-duty hybrid electric vehicle (HEV) where the power demanded by the battery pack is specified prior to downsizing. A calibrated electro-thermal model and a semi-empirical capacity fade model are used to capture voltage, state-of-charge, temperature and capacity loss of the downsized battery. The capacity fade model is developed based on a novel set of experiments designed to clarify the influence of nominal operating SOC on battery degradation. The parametric study shows that the pack size could be reduced from 76 to 64 cells while shifting nominal operating SOC from 50% to 35% without experiencing battery power denials. This would result in a 20% increase in energy utilization per cell, with only a 0.4% increase in capacity fade.**

I. Introduction

Hybrid Electric Vehicle (HEV) manufacturers seek to reduce the weight and cost of their vehicles to gain competitive advantage. Mainly this could be achieved by reducing the weight and/or size of the engine or battery pack in the vehicle. In this paper the emphasis on downsizing is shifted from the engine to the battery assuming a fixed engine and vehicle power management.

Battery downsizing will increase the energy throughput and the root mean square (RMS) currents, generating more heat and triggering potentially more often the operational voltage limits. Therefore, to guarantee safe operation and extend battery life, power input or output from the battery should be regulated within specified limits. More importantly, the battery power limits, or charge/discharge power capabilities depend on the nominal SOC operating window. In most commercial HEVs' the nominal SOC operation is centered around 50% or higher which allows for more discharge and thus higher power capabilities and battery efficiencies. Using dynamic models and predictive battery management techniques, this paper provides a case study on battery downsizing and SOC operating window for an existing light-duty vehicle.

Much effort has been expended to accurately compute power capability of batteries in real-time [1]–[4] wherein electrical, electrochemical, and thermal constraints such as terminal voltage, battery SOC, Li-ion concentration, and temperature are considered. These algorithms effectively regulate battery operation, that is, none of the considered constraints are violated during battery operation. As the 2nd generation Li-ion powered HEVs are being designed and about to appear in the market, the influence on the battery performance (e.g. utilization, temperature, and life) associated with battery sizing and operating SOC window needs to be thoroughly studied. Therefore, this paper investigates various performance metrics of the battery operation with a model-based power limiting approach in an HEV application.

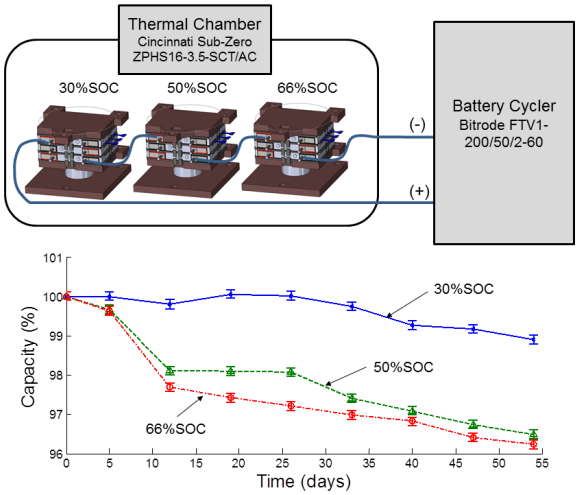

Fig. 1. Setup and results of experimental capacity fade testing at different SOCs

To quantitatively study the performance of a battery, it is essential to have accurate representation of the internal dynamics of the battery, i.e. electrical/thermal behavior and capacity fading. To that end, an equivalent-circuit model, a lumped thermal capacitance model [5], and a semi-empirical capacity fade model [6] are integrated in this work to capture terminal voltage, battery state-of-charge (SOC), temperature, and capacity loss, respectively. In particular, the capacity fading model is parameterized using a novel set of experiments that highlight the influence of nominal operating SOC on

978-1-4673-7637-2/15/$31.00 ©2015 IEEE

degradation as shown in Fig. 1. Such models have been widely used and have shown to be sufficient for performance computation in automotive applications. In investigating downsizing of a battery pack, an actual current profile from the battery pack equipped with Ford's HEV is used. The profile assumes a fixed engine and vehicle power management and is scaled as number of cells is changed to match the total power demanded or supplied.

The main contribution of this paper is to investigate the influence of battery pack downsizing, more specifically reducing battery count, and shifting the center of nominal operating SOC window to the battery performance in an HEV application. Here we define a power denial as requested batter power greater than the limit set by the control algorithm. The parametric study shows that the battery pack under consideration can be scaled down from 76 to 64 cells without experiencing any discharge power denials when nominal operating SOC is shifted from 50% to 35%. Each cell in the pack would experience a 20% increase in energy utilization with only a 0.4% capacity fade increase.

II. Predictive Battery Models

The objective of this study is to quantitatively analyze the performance of a Li-ion battery under a model-based power limiting method in HEV application. To this end, a model is essential to accurately capture the electrical/thermal dynamics and capacity fading of the battery.

A. Electro-thermal model

In this study, a prismatic Nickel–Manganese–Cobalt (NMC)/Graphite Li-ion cell is used. The cells were extracted from a 2013 Ford Focus HEV battery pack. The cell and pack specifications of the HEV are provided in Table I.

1) Electrical model: The electrical dynamics of the battery are captured by using an OCV-R-2RCs model. The model is mathematically represented by

$$\begin{bmatrix} \dot{V}_1 \\ \dot{V}_2 \\ \dot{z} \end{bmatrix} = \begin{bmatrix} \frac{-1}{R_1 C_1} & 0 & 0 \\ 0 & \frac{-1}{R_2 C_2} & 0 \\ 0 & 0 & 0 \end{bmatrix} \begin{bmatrix} V_1 \\ V_2 \\ z \end{bmatrix} + \begin{bmatrix} \frac{1}{C_1} \\ \frac{1}{C_2} \\ -\frac{1}{Q} \end{bmatrix} I, \quad (1)$$
$$V_t = V_{\text{oc}}(z) - V_1 - V_2 - R_s I,$$

where Q is the nominal capacity of the cell and I is the current across it. The polarization voltages, V_1 and V_2, are the voltages across the RC pairs, $\{R_1, C_1\}$ and $\{R_2, C_2\}$, respectively, and z is the SOC of the cell. The electrical resistances, R_s, R_1 and R_2, and the capacitances, C_1 and C_2, are parameterized using voltage responses when the battery is excited by current pulses at different SOCs and temperatures as described in [5].

TABLE I
Specifications of battery cell and pack from Ford's HEV

Cell	Value
Nominal Capacity	5 Ah
Nominal Voltage	3.7 V
Dimension	120 × 85 × 12.7 mm
Pack	**Value**
Number of Arrays	2
Number of Cells in Parallel	1
Number of Cells in Series	76

When the battery power, P_b, is given, the following equation is used to compute the battery current:

$$I = \frac{V_{\text{oc}} - V_1 - V_2 - \sqrt{(V_{\text{oc}} - V_1 - V_2)^2 - 4R_s P_b}}{2R_s}. \quad (2)$$

2) Thermal model: The thermal dynamics are captured by a lumped capacitance model with one temperature representing the cell, T. The heat equation governing the thermal model with convection cooling is given by

$$mc_p\dot{T} = \dot{Q}_{\text{gen}} + hA(T_\infty - T), \quad (3)$$

where m is the mass of the cell and c_p is the lumped heat capacity. The heat dissipation by convection is influenced by the heat transfer convection coefficient, h, the surface area of the cell, A, and the temperature difference between the cell and the ambient, T_∞. The heat generation, $\dot{Q}_{\text{gen}}$, is determined by the electrical model and is defined as

$$\dot{Q}_{\text{gen}} = I^2 R_s + \frac{V_1^2}{R_1} + \frac{V_2^2}{R_2} - IT\frac{dU}{dT}, \quad (4)$$

where $\frac{dU}{dT}$ is a change in OCV with respect to a change in battery temperature and is related to the entropy change in the battery, a certain amount of energy to balance the whole reactions inside the battery. The first three terms of Eq. (4) represent the ohmic heat generation while the last term of Eq. (4) represents the entropic heat generation in the cell.

B. Capacity Fade Model

To predict capacity fade of the battery, a semi-empirical model, which has been widely used in literature [6]–[8], is adopted. A capacity fade model uses a power law with Arrhenius relation in order to relate stress factors such as charge throughput (Ah) and temperature to capacity fade. In [6], nominal operating SOC is considered as another stress factor.

However, the model cannot be applied without modifications since the chemistries of the battery in this study are not the same. Therefore, the slightly modified model is parameterized against experimental data. Experiments are performed using continuous charge sustaining current profiles. These current profiles are obtained by Eqs. (1) and (2) by applying the battery power input from Ford's HEV over US06 cycle on three cells with three different nominal SOCs (33%, 50% and 66%)[1]. Data is collected for 56 Kmiles or an equivalent 36 KAh.

The temperature of the battery at quasi steady state is regulated at 25°C; the ambient temperature is controlled at 10°C. The experimental procedure is as follows:

[1]The power management system in HEV typically regulates battery pack's SOC around the center of an operating window; however, this does not necessarily mean that the average SOC is at the center value of the target SOC operating window. In our work, power demand is the input without any SOC regulation, therefore the term *nominal SOC*, is used to refer to the initial SOC and not the average operating SOC.

- Cycle cells continuously using a US06 cycle for 900 cycles [corresponding to 7.2 Kmiles or 4.6 KAh].
- Charge cells using a CCCV (constant-current constant-voltage) protocol to 4.1 V (100% SOC) at 1C rate. Rest for 24 hrs.
- Discharge cells to 2.9 V (0% SOC) at 1C rate.
- Measure and record discharge capacity.

Figure 1 shows a schematic of the setup used for capacity testing of the cells along with the results of capacity fading. The cells are connected in series so that the same current is applied to all of them and placed in a thermal chamber for ambient temperature control. They are clamped and constrained similar to what they would experience in the battery pack. Note that the degradation testing also resulted in a general overall increase of 2% in series resistance R_s. This increase, however, has large variance, and therefore more miles of degradation testing is needed to quantify the trend of resistance degradation and come up with a suitable model for it. Thus resistance degradation is not considered in this study and is assumed not to affect the power capability of the cell. For a more conservative design of pack, the resistance increase after 100,000 miles[2] has to be considered instead.

The choice of the driving cycle and nominal SOCs are deliberate. First, the US06 cycle is the most aggressive standard driving cycle requiring high power demand from/to the battery, which makes the power profile reasonable to investigate the battery performance related to power denials which relates to the drivability of the vehicle. Second, the rate of capacity fade is accelerated when operating around high stress and SOC [9], [10]. Authors in [11] observed that bulk force of constrained batteries increased with respect to increasing SOC. Particularly, phase changes of materials in the negative electrode could be observed: below 50% SOC, between 50 and 80% SOCs and above 80%. Considering typical SOC range of HEVs and the phase changes of the electrode materials of the battery, three nominal SOCs are selected.

The following empirical model is used to predict capacity loss,

$$S_{\text{loss}} = \left(\alpha_c + \gamma_c(0.66 - \text{SOC}_0)^c\right) \cdot \exp\left(\frac{-E_{\text{ac}}}{R_{\text{g}}T}\right) \cdot \text{Ah}^{\xi}, \quad (5)$$

where S_{loss} is the capacity fade in percentage, SOC_0 is the nominal SOC, $\text{SOC}_0 \in [0.33, 0.66]$, Ah is the charge throughput, R_{g} is the universal gas constant, 8.314 J/Kmol, and T is the cell temperature. Note that, due to lack of sufficient data to reflect the influence of temperature, the activation energy E_{ac} is assumed to be the same as the value in [6][3], 22406 J/mol. Identified constants, α_c, γ_c, c, ξ, E_{ac} and R_{g}, are listed in Table II.

The performance of the capacity fade model is shown in Fig. 2 by comparing with experimental data.The model would allow for capacity calculation up to 100,000 miles for the different operating nominal SOCs and temperatures.

[2]Automakers such as Nissan, Chevrolet, Toyota and Ford guarantee their battery packs for at least either 8 years or 100,000 miles whichever comes first.

[3]The chemistries of batteries in [6] are NMC-LMO/graphite.

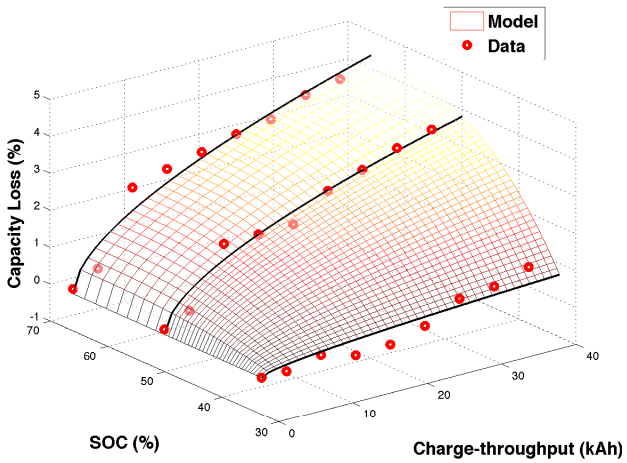

Fig. 2. A capacity fade model with experimental data

TABLE II
CONSTANTS FOR THE CAPACITY FADE MODEL EQ. (5)

Constant	α_c	γ_c	c	ξ	E_{ac}	R_{g}
Value	125.2	-1925	2.618	0.5361	22406	8.314

III. PULSE POWER CAPABILITY COMPUTATION

In determining model-based power capability, voltage and SOC constraints are considered independently based on time-scale separation. The model-based power capability is typically determined by computing limiting current and projected terminal voltage to avoid computational burden. To solve each constraint problem, a simple method described in [2] is adopted to compute the maximum current ensuring that no constraints are violated. This method is based on iteration and inversion of a dynamic model by receding horizon scheme.

Consider a linearized discrete-time electrical model, Eq. (1), whose dynamics are described by the following set of difference equations

$$x_{k+1} = Ax_k + BI_k,$$
$$y_k = Cx_k + DI_k + F,$$

where system matrices associated with the output, y, are denoted by A, B, C, D and F[4]. For a constant current input $\bar{I}$, the state x and output y after N future steps are given by

$$x_{k+N} = A^N x_k + \sum_{i=0}^{N-1} A^i B\bar{I},$$
$$y_{k+N} = Cx_{k+N} + D\bar{I} + F.$$

Therefore, at any instant k, the maximum permissible current that does not violate a constraint $\bar{y}$ on the output y in N future

[4]Matrices for the electrical system are obtained through linearization and discretization processes around the operating point at each sampling time

steps is determined by

$$\bar{I} = \left(\sum_{i=0}^{N-1} CA^i B + D \right)^{-1} \left(\bar{y} - CA^N x_k - F \right).$$

Finally, the power capability, $\bar{P}_\mathrm{b}$, is computed by the product of the maximum permissible current and terminal voltage after N future steps expressed as

$$\bar{P}_\mathrm{b} = \bar{I} \cdot V_{\mathrm{t},k+N|k},$$

where the predicted terminal voltage $V_{k+N|k}$ is calculated with

$$\begin{aligned} V_{\mathrm{t},k+N|k} = V_\mathrm{oc} \left(z_k - \frac{N\Delta t \bar{I}}{C_\mathrm{b}} \right) - R_{\mathrm{s},k} \bar{I} \\ - e^{\frac{-N\Delta t}{R_{1,k} C_{1,k}}} V_{1,k} - R_{1,k} \left(1 - e^{\frac{-N\Delta t}{R_{1,k} C_{1,k}}} \right) \bar{I} \\ - e^{\frac{-N\Delta t}{R_{2,k} C_{2,k}}} V_{2,k} - R_{2,k} \left(1 - e^{\frac{-N\Delta t}{R_{2,k} C_{2,k}}} \right) \bar{I}. \end{aligned}$$

where Δt is a sampling period. For more detailed description about the method including how to handle nonlinearities in thermal dynamics, the interested reader is referred to [2]. In this study, terminal voltage and SOC are chosen as constraint parameters, i.e., $\bar{y} \in \{V_\mathrm{min}, V_\mathrm{max}, \mathrm{SOC}_\mathrm{min}, \mathrm{SOC}_\mathrm{max}\}$.

IV. Simulation Results

Quantitative analysis on battery performance is conducted by testing the battery model and the power limiting method described before with the simulated US06 power input at various operation conditions: (1) ambient temperatures, $T_\infty \in \{-5, 25\}^\circ$C; (2) nominal SOCs, $\mathrm{SOC}_0 \in \{0.35, 0.4, 0.45, \cdots, 0.65\}$; and (3) number of cells in a battery pack, $N_b \in \{48, 50, \cdots, 76\}$. These changes in operating conditions affect the battery performance such as battery utilization, average current, temperature rise, and capacity fade. As the battery size changes, the battery power per cell is scaled correspondingly to provide the same power. The limits on voltage and SOC for the power limiting algorithm are shown in Table III. Note that the SOC limits define a window of 40% SOC operating range. All results in this section are based on cell level and not pack level.

To provide a better understanding, time series plots of power, voltage, SOC and temperature at 35% SOC, $T_\infty = 25^\circ$C and $N_b = 64$ are shown in Fig. 3, as an example. The first subplot shows a scaled (by a factor of 1.2) simulated battery power associated with US06 drive cycle, and the discharge (+) and charge (-) power limits for one cell in the $N_b = 64$ cell pack. These power limits vary because the battery's internal states and parameters change. Note that the actual power input to the battery is clamped by these two limits. The first subplot also shows instances (highlighted in green circles) where the power input to the battery exceeds the power limits. The first two circles at $t = 20$ sec and $t = 120$ sec show instances where the lower and upper voltage limits respectively are reached and so power is clamped. Moreover, the third and fourth circles show instances where the lower SOC limit is reached and, thus, also the power limit is clamped. These violations represent missed energy opportunities that the cell could have provided. For this case of $N_b = 64$ cells in the pack, since the battery power input is increased, the cell needs to provide more power and current when compared to the baseline case ($N_b = 76$ or power factor = 1). Thus, changes in total energy-throughput, root-mean-square averaged current and temperature rise can also be determined. Apart from potential power denial concerns, the total energy-throughput during power denials – where the magnitude of battery power is greater than or equal to power capability – is of interest because this number would be related to fuel consumption, i.e. the supervisory controller in the HEV will increase the power demand from the engine.

TABLE III
Upper and Lower Limits on Voltage and SOC

Output	Lower/Upper Bound	Unit
Voltage	2.5/4.1	V
SOC	$\mathrm{SOC}_0 \pm 0.2$	–

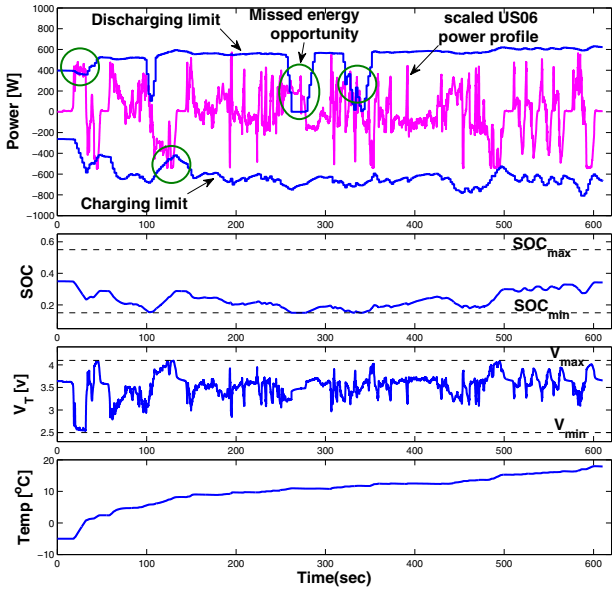

Fig. 3. Power, SOC, voltage, and temperature profiles at 35% SOC, $T_\infty = -5^\circ$C and number cells = 64

Simulation results of the parametric study for one cell in a pack of N_b cells are plotted in Fig. 4. The energy-throughput utilization (upper left), temperature increase (upper right), RMS current (lower left) and unavailable discharge energy (lower right) are plotted as a function of nominal SOC and number of cells at an ambient temperature of $T_\infty = 25^\circ$C. The unavailable discharge energy (UDE) is computed by

$$\mathrm{UDE} = \sum \max\{P_\mathrm{b,dmd} - \bar{P}_\mathrm{b}^\mathrm{dch}, 0\} \Delta t, \qquad (6)$$

where the battery power demand and maximum discharge power are denoted by $P_\mathrm{b,dmd}$ and $\bar{P}_\mathrm{b}^\mathrm{dch}$, respectively.

All results are computed after completing one simulated US06 power cycle. As expected, results show that as number of cells in a pack are decreased, the energy throughput

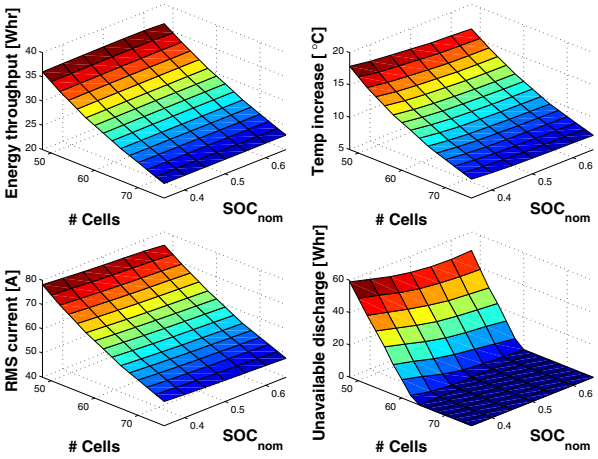

Fig. 4. Energy throughput, temperature, RMS current and unavailable discharge at $T_\infty = 25°\text{C}$

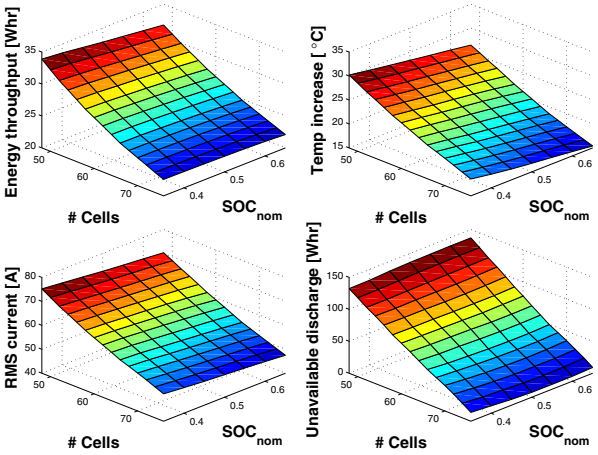

Fig. 6. Energy throughput, temperature, RMS current and unavailable discharge at $T_\infty = -5°\text{C}$

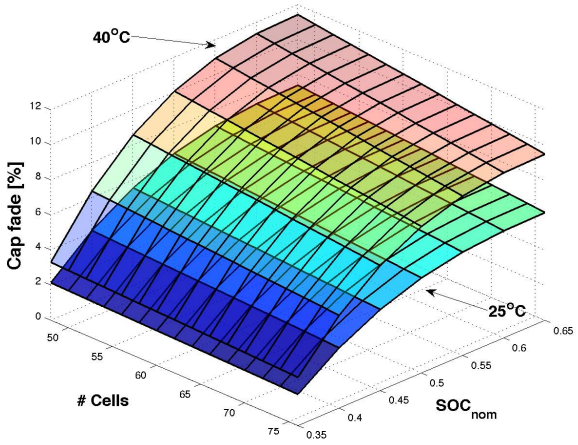

Fig. 5. Capacity fade after 100,000 miles at a cell temperature of 25°C and 40°C

increases. Accordingly, the temperature and RMS current increase as well. More interestingly, the unavailable discharge graph shows that the number of cells in a pack can be scaled down without violating any discharge power constraints. This means that drivability is not affected.

The simulated capacity fade after 100,000 miles of the cell is also shown in Fig. 5. Also, since different number of cells would result in different power factors and thus in different temperature increase in the cell, it has to be assumed that, for capacity fade analysis, the cells are cycled at the same temperature regardless of the how many cells are used. This means, that depending on the number of cells (or power factor), the convection scheme is adjusted so that the equilibrium temperature of the cell is the same. The capacity fade is shown for a temperature of 40°C and 25°C. Figure 5 shows that capacity fade is greatly affected by the nominal operating SOC but not by the number of cells, and is accelerated at higher temperatures.

Figures 4 and 5 together show that the number of cells could be scaled down which results in higher cell utilization and without experiencing any discharge power denials (i.e. unavailable discharge energy throughput is zero). Also, operating the cell at a lower SOC would result in minimal capacity fade after 100,000 miles, even with a smaller number of cells.

Figure 6 shows the resulting energy throughput utilization, temperature increase, root mean square (RMS) current increase and unavailable discharge power as a function of nominal SOC and number of cells at an ambient temperature of $T_\infty = -5°\text{C}$. Results again show that operating at lower SOCs will result in higher cell utilization with minimal discharge power denial even with a scaled down battery pack size (lower number of cells). However, at these low temperatures, the resistance of the battery is large, and thus, even with a full pack ($N_b = 76$ cells), voltage limits are violated and power is clamped. Therefore, as shown in Fig. 6, the unavailable discharge subplot shows that there are no instances where discharge power constraints are not violated.

From Fig. 4, it can be deduced that at 35% SOC (preferable operating SOC in terms of capacity fade), the number of cells could be decreased from 76 to 64 without violating any discharge power constraints. Table IV shows the results of decreasing the number of cells to 64 at a nominal SOC of 35%. Note that the results are for a single simulated US06 power input cycle, except for the capacity fade which is projected at 100,000 miles.

Table IV shows that, for $N_b = 64$ cells, a 20% Whr increase in utilization per cell results only in a 0.4% increase in capacity fade over the lifetime of the battery without

TABLE IV
RESULTS OF BATTERY DOWNSIZING AT $T_\infty = 25°\text{C}$ AND 35% SOC

Number Cells	76	64	Change
Energy utilization [Whr]	22.99	27.52	+20 %
Temperature increase [°C]	7.92	11.05	+3°C
RMS current [A]	49.99	59.74	+20 %
Denials [sec]	0	0	–
Capacity fade [%]	3.54	3.89	+0.4 %

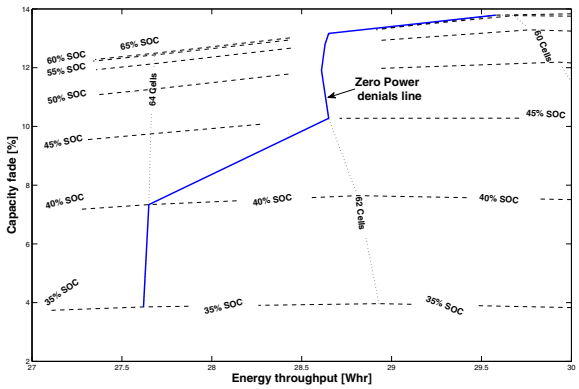

Fig. 7. Zero power denials plot of capacity fade after 100,000 miles vs. energy-throughput per cell at $T_\infty = 25^\circ$C.

experiencing any discharge power denials (violating discharge power constraints) as compared to a base case of $N_b = 76$. The RMS current also increases because of higher power request, and accordingly, the temperature of the cell also increases.

A zero power denials line could be extracted from Fig. 4. This line defines the minimum number of cells at each SOC for which the cell can provide full discharge power. Figure 7 shows the zero power denials line on a plot of capacity fade versus energy throughput per cell. In order for the pack to deliver full discharge power, the operating point has to be above the zero power denials line, meaning there are no violations of the discharge power constraints. The plot shows that for low energy throughput, operation could be around any SOC. As the number of cells is decreased, the energy throughput per cell is increased. Accordingly, for zero power denials, the operating SOC has to be increased. That would also increase the capacity fading in the cell. However, if the capacity fade after 100,000 miles is less than that specified by the manufacturer warranty, then the number of cells can be significantly decreased in a hybrid pack while experiencing zero power denials.

V. Conclusions

This paper presents an opportunity to downsize a Ford HEV pack from 76 cells to 64 cells without experiencing any power denials and with only a 0.4% increase in capacity fade. The effect of varying nominal operating SOC and the number of cells in the pack on the performance of the Li-ion batteries was considered. Specifically, performance metrics including energy-throughput utilization, temperature increase, RMS current, unavailable discharge energy and capacity fade were considered for a quantitative analysis.

A predictive thermo-electric model and a semi-empirical capacity fade model were used to capture SOC, voltage, temperature and capacity fade of the Li-ion cells under consideration. Particularly, the capacity fading model was parameterized using data collected from a novel set of experiments for the NMC chemistry in which an actual power profile from the HEV over an aggressive federal driving schedule, US06, was used. A zero power denials plot was created to identify regions of zero power denials (no violations of discharge power denials) as a function of nominal operating SOC, capacity fade and energy throughput per cell.

Future work would include the effect of resistance increase due to degradation and looking at the performance of the cells at different temperatures, especially at low temperatures where performance is limited.

VI. Acknowledgment

The information, data, or work presented herein was funded in part by the Advanced Research Projects Agency-Energy (ARPA-E), U.S. Department of Energy, under Award Number DE-AR0000269[5]. The authors would like to acknowledge the contribution of Dyche Anderson from Ford Motor Company and Aaron Knobloch from GE Global Research.

References

[1] R. D. Anderson, Y. Zhao, X. Wang, X. G. Yang, and Y. Li, "Real time battery power capability estimation," in *Proceedings of the American Control Conference*, June 2012, pp. 592–597.

[2] Y. Kim, S. Mohan, J. B. Siegel, and A. G. Stefanopoulou, "Maximum power estimation of lithium-ion batteries accounting for thermal and electrical constraints," in *Proceedings of ASME Dynamic Systems Control Conference*, Palo Alto, California, USA, Oct 22-24 2013, p. V002T23A003.

[3] H. Perez, N. Shahmohammadhamedani, and S. Moura, "Enhanced performance of li-ion batteries via modified reference governors and electrochemical models," *Mechatronics, IEEE/ASME Transactions on*, vol. PP, no. 99, pp. 1–10, 2015.

[4] K. Smith, C. Rahn, and C.-Y. Wang, "Model-based electrochemical estimation and constraint management for pulse operation of lithium ion batteries," *Control Systems Technology, IEEE Transactions on*, vol. 18, no. 3, pp. 654–663, 2010.

[5] N. A. Samad, J. B. Siegel, and A. G. Stefanopoulou, "Parameterization and validation of a distributed coupled electro-thermal model for prismatic cells," in *2014 ASME Dynamic Systems and Control Conference*, 2014.

[6] A. Cordoba-Arenas, S. Onori, Y. Guezennec, and G. Rizzoni, "Capacity and power fade cycle-life model for plug-in hybrid electric vehicle lithium-ion battery cells containing blended spinel and layered-oxide positive electrodes," *Journal of Power Sources*, vol. 278, no. 0, pp. 473 – 483, 2015.

[7] J. Wang, P. Liu, J. Hicks-Garner, E. Sherman, S. Soukiazian, M. Verbrugge, H. Tataria, J. Musser, and P. Finamore, "Cycle-life model for graphite-lifepo4 cells," *Journal of Power Sources*, vol. 196, no. 8, pp. 3942 – 3948, 2011.

[8] J. Wang, J. Purewal, P. Liu, J. Hicks-Garner, S. Soukazian, E. Sherman, A. Sorenson, L. Vu, H. Tataria, and M. W. Verbrugge, "Degradation of lithium ion batteries employing graphite negatives and nickel-cobalt-manganese oxide + spinel manganese oxide positives: Part 1, aging mechanisms and life estimation," *Journal of Power Sources*, vol. 269, no. 0, pp. 937 – 948, 2014.

[9] J. C. Forman, S. J. Moura, J. L. Stein, and H. K. Fathy, "Optimal experimental design for modeling battery degradation," in *2012 ASME Dynamic Systems and Control Conference; Ft. Lauderdale, FL*, 2008.

[10] M. T. Lawder, P. W. C. Northrop, and V. R. Subramanian, "Model-based sei layer growth and capacity fade analysis for ev and phev batteries and drive cycles," *Journal of The Electrochemical Society*, vol. 161, no. 14, pp. A2099–A2108, 2014.

[11] Y. Kim, S. Mohan, N. Samad, J. Siegel, and A. Stefanopoulou, "Optimal power management for a series hybrid electric vehicle cognizant of battery mechanical effects," in *American Control Conference (ACC), 2014*, June 2014, pp. 3832–3837.

[5] Disclaimer: The information, data, or work presented herein was funded in part by an agency of the United States Government. Neither the United States Government nor any agency thereof, nor any of their employees, makes any warranty, express or implied, or assumes any legal liability or responsibility for the accuracy, completeness, or usefulness of any information, apparatus, product, or process disclosed, or represents that its use would not infringe privately owned rights. Reference herein to any specific commercial product, process, or service by trade name, trademark, manufacturer, or otherwise does not necessarily constitute or imply its endorsement, recommendation, or favoring by the United States Government or any agency thereof. The views and opinions of authors expressed herein do not necessarily state or reflect those of the United States Government or any agency thereof.